scientific reports

Check for updates

OPEN

A fundamentally new direction in embolization using reactive chemistry in a swine model

Erik Cressman[1]✉, Danielle Stolley[2], Shubhneet Warar[1], Natalie W. Fowlkes[3] & David Fuentes[4]

Liver cancer carries a poor prognosis and incidence continues to increase. The main therapy for unresectable disease > 3 cm in diameter is Transarterial Chemoembolization. Unfortunately, overall survival for these patients has improved little in the past two decades. To address this, we propose a new approach using a chemical reaction in situ. We report here our results in a pilot study using a swine model. Domestic swine (*n* = 3) were treated in the liver with dichloroacetic anhydride in ethiodized oil. CT imaging was followed 24 h after the procedure by necropsy, histopathology, and mass spectrometry imaging. Animals tolerated the procedure well. Imaging showed that the solution remained stable over 24 h. Areas of coagulative necrosis were identified at histopathology. Multiplex immunofluorescence showed focal areas where antibodies did not bind. Similarly, mass spectrometry imaging showed areas of low-abundance or absent molecular ions and new molecular ions in treated areas. The data presented here provide the first direct evidence that reactive embolization results in fundamental changes in tissue architecture down to the molecular level, suggesting significant therapeutic potential. These encouraging results open a wide new field of image-guided in vivo chemistry worthy of further exploration.

Keywords Hepatocellular carcinoma, Liver Cancer, Transarterial chemoembolization, Covalent modification, Image-Guided chemistry

Many patients with hepatocellular carcinoma, (HCC, liver cancer) present with late-stage disease, for which curative surgery, ablation, or liver transplant are not viable options. Surveillance programs to identify and treat HCC in its early stages, when liver function is well-preserved and outcomes are most favorable, have faced many challenges educating, identifying, and enrolling the population at risk. As a result, screening programs have not had the impact on public health that might be anticipated[1,2]. Due to the increasing global incidence and poor prognosis for HCC, there is much ongoing effort to improve therapy for this disease.

Compared with best supportive care, several emerging therapies may improve the overall survival of appropriate HCC patients[3,4]. For example, the combination of atezolizumab and bevacizumab can provide a survival improvement over monotherapy with sorafenib[5]. Unfortunately, this and other immunotherapies still face many obstacles to broad clinical adoption, notably cost, overall safety, efficacy, and tolerability. Eliciting immunotherapy responses in HCC patients has proven challenging[6–9]. Similarly, advances in radiotherapy for HCC have been slow for many years. Progress has been made more recently with selective stereotactic beam radiation therapy, but evidence is limited, and it is not yet accepted as a part of standard treatment algorithms for HCC. Advances in another variation of transarterial embolotherapy, selective internal radiation therapy with yttrium-90 (particularly higher doses and accurate dosimetry), have only recently begun to influence the therapeutic landscape[10,11]. However, this therapy is not widely available worldwide, and results vary widely based on local expertise.

A more readily available and frequently utilized option for HCC is transarterial chemoembolization (TACE), in which a large but localized dose of drug is delivered as a metastable emulsion precisely into a tumor's blood supply along with embolic material to block blood flow. TACE is historically the mainstay of treatment for unresectable disease without vascular involvement in patients with preserved liver function (Barcelona Clinic Liver Cancer stage A/B)[12]. Some studies in humans have supported the notion that ethiodized oil used in

[1]Department of Interventional Radiology, The University of Texas MD Anderson Cancer Center, Houston, TX, USA. [2]Flow Cytometry & Cellular Imaging Core Facility, The University of Texas MD Anderson Cancer Center, Houston, TX, USA. [3]Department of Veterinary Medicine and Surgery, The University of Texas MD Anderson Cancer Center, Houston, TX, USA. [4]Department of Imaging Physics, The University of Texas MD Anderson Cancer Center, Houston, TX, USA. ✉email: ecressman@mdanderson.org

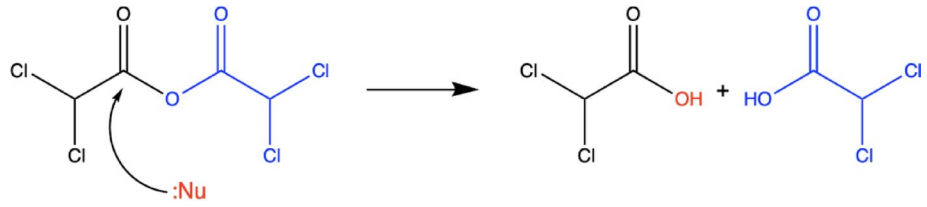

Fig. 1. The proposed reaction of dichloroacetic anhydride in tissue. In the presence of water, the anhydride yields two equivalents of dichloroacetic acid. This protonates and denatures surrounding proteins, causing coagulative necrosis and yields dichloroacetate.

Fig. 2. Angiography of the reactive chemistry embolization procedure. (**A**) Pre-treatment mapping angiogram. Yellow arrow indicates location of microcatheter in **B**. GDA, gastroduodenal artery; SplA, splenic artery. (**B**) Magnified selective angiogram of the target branches of left hepatic artery. (**C**) Post-treatment completion angiogram showing the cessation of antegrade flow in the left hepatic artery (pink arrow). At angiography, the initial rapid flow of droplets of reactive embolic solution decreased within a very short time span (seconds to minutes). This behavior contrasts with drug emulsions, which without an embolic may continue forward flow.

TACE and visualized at CT imaging serves as a prognostic marker; however, these studies lacked pathological validation[13]. Animal studies with pathological validation, in contrast, showed no correlation between the ethiodized oil from the residual emulsion and distribution of the drug delivered[14]. Over the past 20 years, TACE and locoregional drug delivery technology have evolved; for example, TACE can now be performed with drug-eluting beads (DEB-TACE). In spite of such technical developments, TACE alone has not significantly improved overall survival since the initial trials, and DEB-TACE has delivered no additional improvement over conventional TACE[15–17]. A potentially more promising option is balloon-occluded TACE, which provides an element of vascular isolation and control of perfusion not possible with conventional TACE[18,19]. In light of the overall situation, combinations of TACE with other therapies are also being pursued. For example, TACE plus ablation may improve outcomes compared with TACE alone[20], but this combination has yet to be assessed in a randomized prospective trial as well as increasing risks and costs from two procedures. Combinations of TACE with various immunotherapies are also under active investigation[21].

Regardless of the type of transarterial therapy, 50–90% of explanted patient specimens have viable tumor despite imaging showing a complete response. Importantly, this rate has not changed appreciably for years[22–24]. Given these considerations, new, more effective approaches to embolotherapy are clearly needed. Such approaches should expand beyond mechanical changes or changing to the latest drug. After decades of incremental improvements, a fundamentally new direction is required.

Herein, we report our initial efforts using reactive chemistry to perform embolization with dichloroacetic anhydride in a swine model. Reactive embolization simultaneously exerts 3 severe stresses in a highly localized context: ischemia, hyperthermia, and a significant drop in pH. An added benefit of using dichloroacetic anhydride is the creation of a local reservoir of the reaction product dichloroacetate (Fig. 1). This drug has anti-tumor effects through its ability to inhibit pyruvate dehydrogenase kinase, blocking aerobic glycolysis[25]. In the present study, using multiple modalities, we demonstrate the persistence of the embolic solution in the target area for 24 h and its effects on tissues.

Results

Digital Subtraction Angiography (DSA)

DSA performed before the procedure demonstrated typical anatomy with the patency of all major vessels and the absence of any congenital malformations or shunts (Fig. 2A). The similarity of the swine celiac arterial anatomy to the human celiac arterial anatomy was apparent. However, the disposition of the liver lobes and spleen in swine differs from that in humans, with both organs typically spanning the width of the abdomen. This accounts

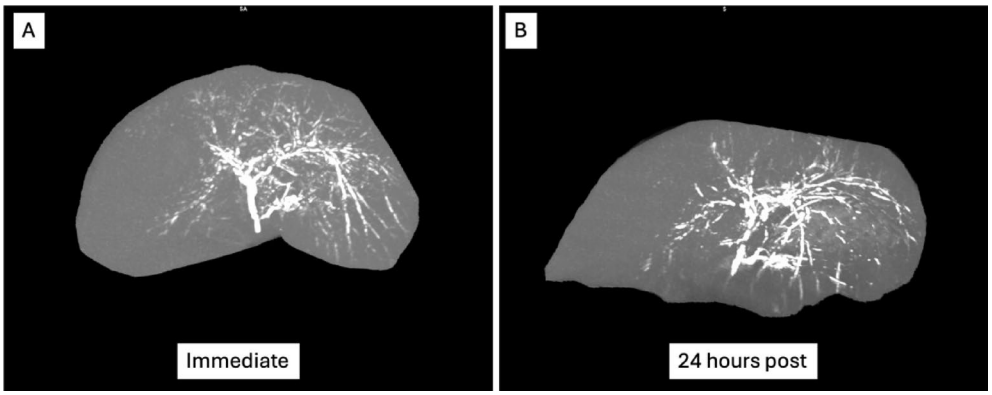

Fig. 3. Three-dimensional volume renderings from CT data demonstrate the persistence of the embolic material in the treatment bed over 24 h. (**A**) Post-processed image from CT acquired immediately after the procedure. (**B**) Post-processed image from CT acquired the following day.

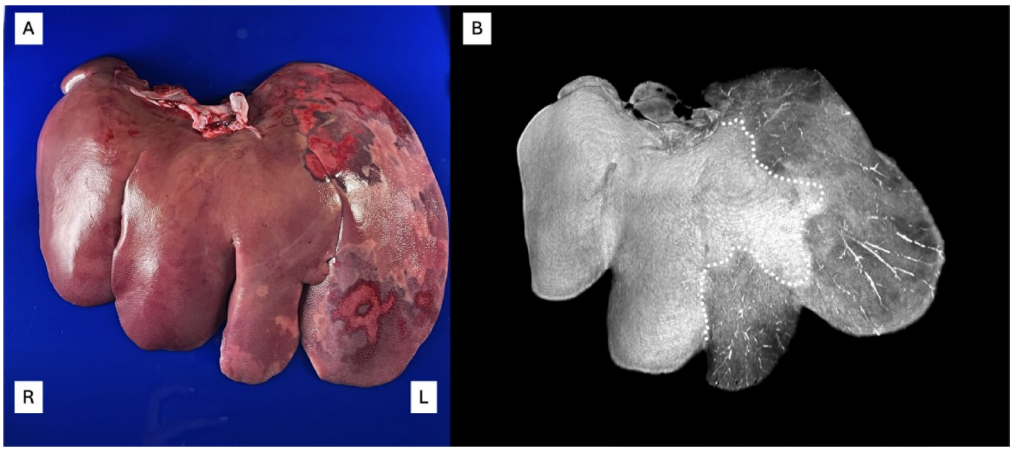

Fig. 4. Whole liver findings at necropsy 24 h after treatment. (**A**) A photograph (dorsal view) of the gross specimen shows extensive damage in the left liver, which has a mottled appearance and multiple focal areas of subcapsular hemorrhage. (**B**) A 3-dimensional volume rendering from CT of the same necropsy specimen in the same orientation. Dotted white line indicates perfusion margin.

for the relatively long common hepatic artery that gives rise to the gastroduodenal artery and vessels supplying the liver, gallbladder, and a portion of the stomach. In many swine, the hepatic artery branches immediately after the gastroduodenal artery, such that no proper hepatic artery is present. During the procedure, the embolic solution was delivered as small aliquots through a microcatheter in the left hepatic artery (Fig. 2B). Digital subtraction angiography performed after the procedure (Fig. 2C) showed stasis of the left hepatic artery with contrast clearly terminating in the stump of the vessel. Subtraction artifacts in a curving pattern just beyond the stump indicated the location of a portion of the embolic solution in the proximal aspect of the left hepatic artery. There was no arterial perfusion in the left lobes of the liver following treatment.

Computed tomography imaging

Non-contrast CT images of the liver were reformatted and sculpted to generate 3-dimensional volume renderings (Fig. 3). These images illustrate the location of the radiopaque embolic solution selectively delivered in the left hepatic arterial tree; no embolic solution was seen on the right side. The solution's distribution immediately after the procedure (Fig. 3A) was similar to its distribution 24 h after the procedure (Fig. 3B). Embolic solution was retained even in the most central branches of the left hepatic artery. For axial non-contrast CT images through liver used for reconstructions see Supplementary Movies S1 and S2, respectively.

Gross pathology

The freshly explanted specimen showed the effects of reactive chemistry embolization with dichloroacetic anhydride (Fig. 4A). The surface of the treated area appeared mottled, notably in the left lateral lobe, with multifocal areas of subcapsular hemorrhage. CT of the explanted liver showed the presence of the embolic solution in the arterial tree and the absence of perfusion in the treated areas (Fig. 4B). Because euthanasia

was performed immediately prior to acquisition of the final triple-phase CT scan, the diffuse, relatively higher attenuation throughout the unaffected, normally perfused liver is likely attributable to residual contrast.

Histopathology

The effects of the reaction of dichloroacetic anhydride in tissue were readily apparent at the microscopic level. H&E staining revealed large areas of coagulative necrosis with relatively sharp margins and hemorrhage in the periphery (Fig. 5A-C). There was preserved architecture at the margins but widespread complete breakdown of cytoskeletal structure deeper within the target zone.

Multiplex immunofluorescence

Multiplex immunofluorescence microscopy revealed focal areas of severe signal depletion for DAPI and for 5 of the 6 antibodies in the panel tested (Fig. 6B-H). These areas corresponded to regions of coagulative necrosis in an adjacent H&E-stained section (Fig. 6A). Only the hepatocyte marker arginase 1 retained a modest residual signal in the damaged areas (Fig. 6H and Fig. 7). A few cells in a narrow band at the outer edge of the most severe damage displayed arginase 1 nuclear staining (Fig. 7C). This staining coincided with the decreased signal in the DAPI channel, but the width of the DAPI fluorescence band was considerably greater and extended deeper into the damage zone before complete loss (Fig. 7B). Vimentin and smooth muscle actin had similar staining patterns (Fig. 7A, E, F), with signal loss at approximately the same depth. CD45 + cells were scattered throughout the specimen and accumulated at the margins of the damaged areas (Figs. 6F and 7D and E). The CD45 positivity in the damage zone was sparse compared with that in the surrounding tissues (Fig. 7D, E). The apoptosis marker cleaved caspase-3 was relatively poorly expressed, with only a few scattered areas of positivity (Fig. 7B, C).

Mass spectrometry imaging

Figure 8 shows a fresh specimen (Figure 8A), an H&E-stained frozen section (Figure 8B), and mass spectrometry images ordered by increasing m/z ratios of the molecular ions (Figure 8C-J). These were chosen to illustrate the broad range of possible scenarios in a specimen, many of which cannot be visualized with any alternate technologies. Negative ion mode images of areas corresponding to the damage seen on both gross examination of fresh specimens and histopathological analysis of frozen specimens reveal clear differences in molecular composition. In the necrotic zone, several molecular ions are either missing altogether or have notably attenuated signal intensity (Figure 8C-E, G, L). By contrast, several molecular ions that are present primarily in the treated areas are effectively absent in the viable, untreated areas (Figure 8F, H-J). Both the treated and untreated areas showed the feature at m/z 778.5082 depicted in Figure 8K suggesting this molecular ion was more stable to the conditions imposed by reactive embolization.

Discussion

The focus of this study was the initial testing of reactive embolization in a small number of animals to assess the performance of dichloroacetic anhydride in vivo. New and more effective treatment options for HCC are clearly needed, and reactive embolization, such as that reported here, may address this need. The deployment,

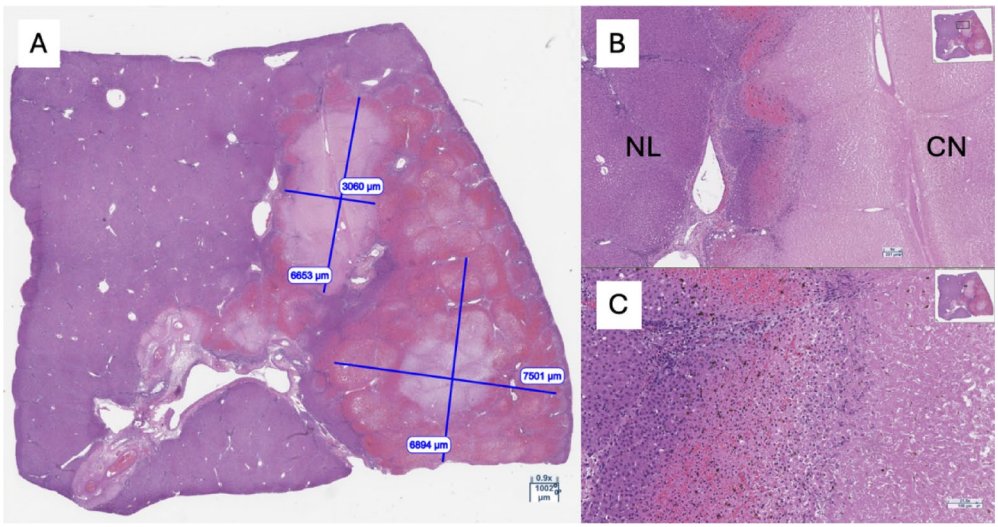

Fig. 5. Histopathology 24 h after reactive chemotherapy embolization with dichloroacetic anhydride. (**A**) A photomicrograph of an H&E-stained tissue section shows multifocal and coalescing areas of extensive necrosis and hemorrhage. The areas of necrosis marked by the blue lines measure 3060 µm x 6653 µm and 7501 µm x 6894 µm, respectively (magnification 1x) (**B**) A photomicrograph shows a sharp border between the area of coagulative necrosis (CN) and normal liver (NL) (magnification 6x). (**C**) A photomicrograph shows that the border is characterized by hepatocytes with pyknosis, karyorrhexis, and karyolysis and by congestion, hemorrhage, and hemosiderin-laden macrophages (magnification 20x).

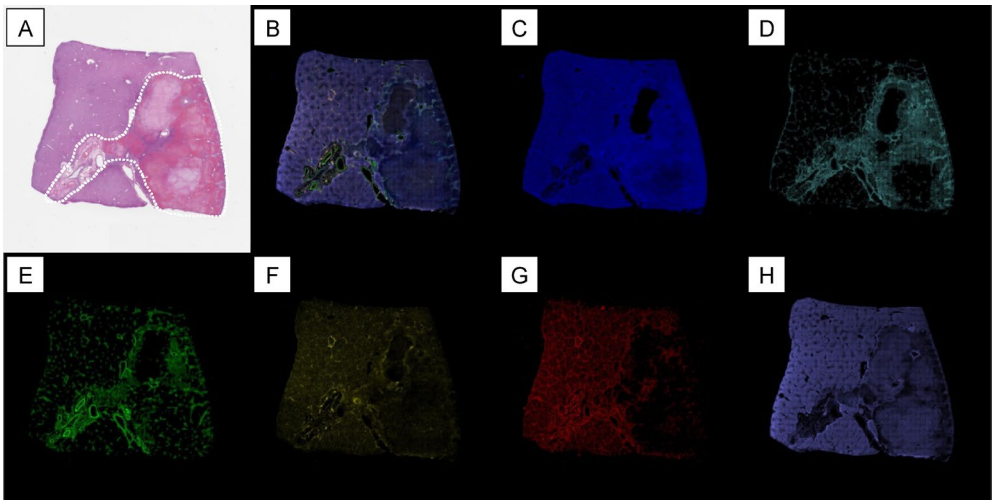

Fig. 6. Multiplex immunofluorescence microscopy. (**A**) An H&E-stained tissue section. Dotted white line indicates area dominated by coagulative necrosis (**B**-**H**). (**B**) An adjacent tissue section shows combined immunofluorescence staining; immunofluorescence staining for (**C**) DAPI; (**D**) vimentin; (**E**) smooth muscle actin; (**F**) CD45; (**G**) CD31; and (**H**) arginase 1. With the exception of arginase 1, all markers have a focal loss of signal in the most severely damaged areas.

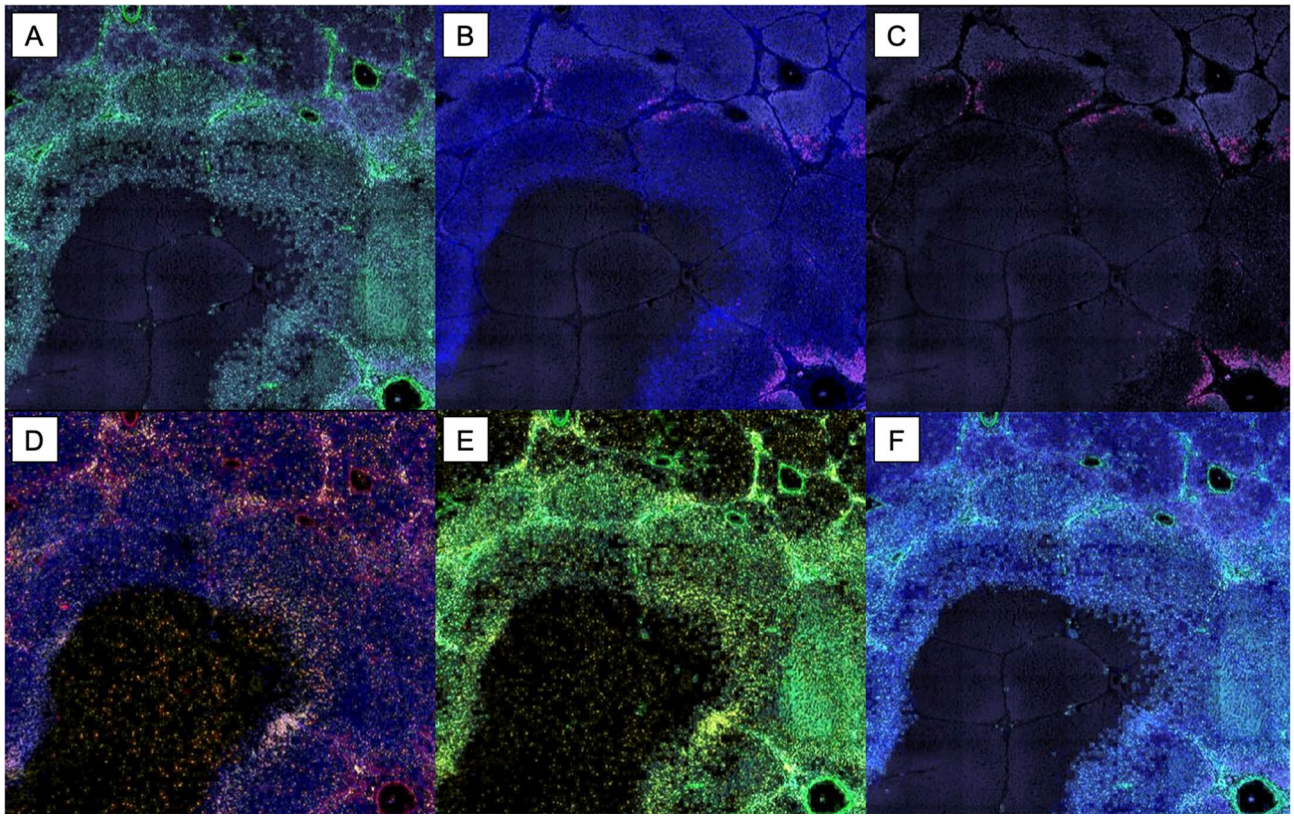

Fig. 7. Multiplex immunofluorescence microscopy. (**A**-**F**) Multichannel images of (**A**) arginase 1, smooth muscle actin, and vimentin; (**B**) arginase 1, DAPI, and cleaved-caspase 3; (**C**) arginase 1 and cleaved caspase 3; (**D**) DAPI, CD45, and CD31; (**E**) vimentin and CD45; and (**F**) DAPI, arginase 1, smooth muscle actin, and vimentin (magnification 4x).

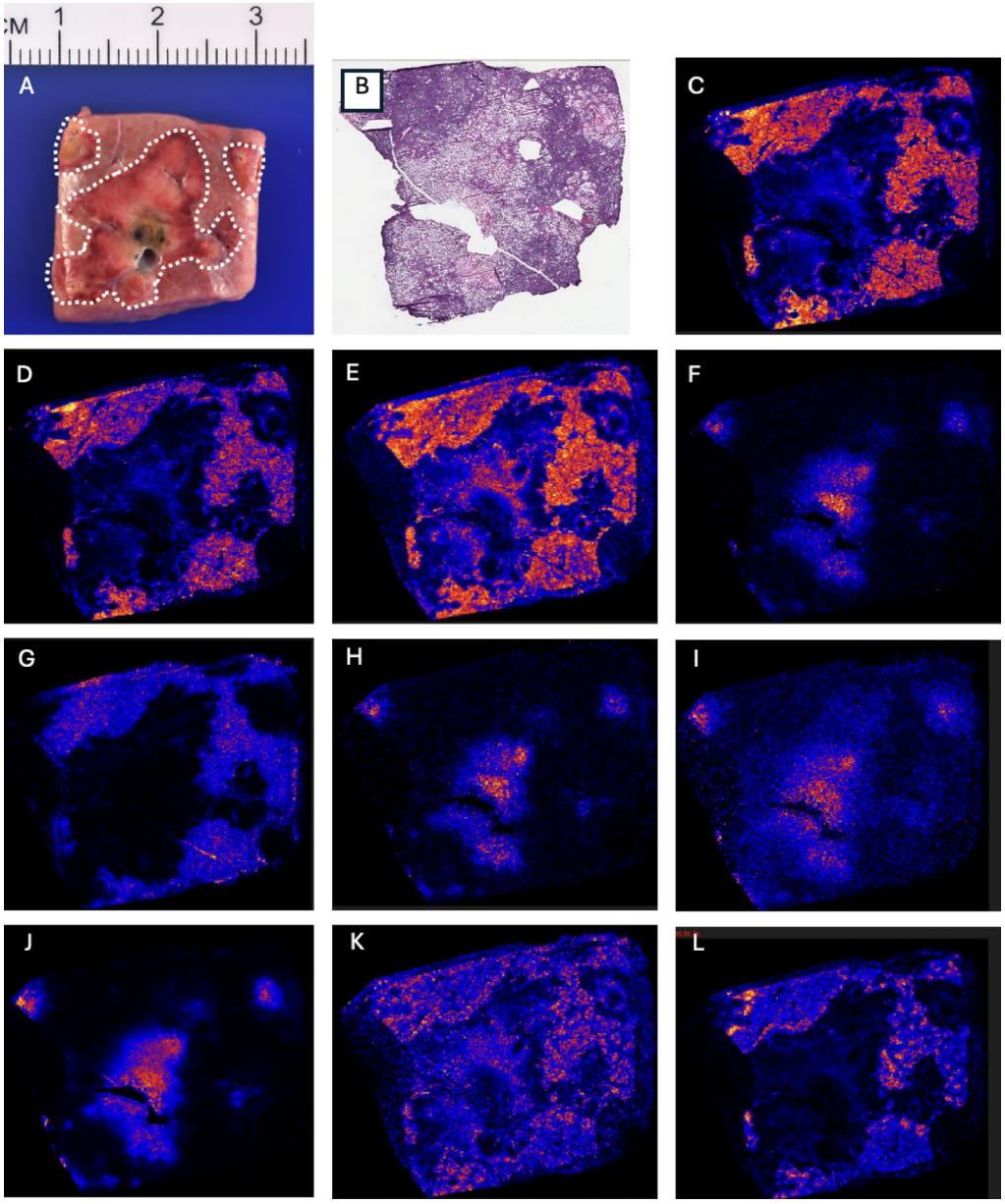

Fig. 8. Mass spectrometry imaging. (**A**) A fresh tissue specimen shows extensive hemorrhagic margins around areas of coagulative necrosis denoted by the dotted white line. (**B**) An H&E-stained frozen section. (**C**-**L**) Molecular ion images of an adjacent tissue section obtained in negative ionization mode in order of increasing m/z values: (**C**) 279.2311; (**D**) 303.2307; (**E**) 419.2531; (**F**) 446.2848; 448.0009; (**H**) 449.3055; (**I**) 494.2589; (**J**) 499.2890; (**K**) 778.5082; and (**L**) 863.5576.

tissue effects, and stability of the material in the target region were of primary importance. Multimodal analyses characterized the damage and the response in greater depth, providing greater insight than that possible with standard histology alone.

Our CT findings showed that the disposition and distribution of ethiodized oil did not change appreciably from immediately after the procedure to 24 h after the procedure. One of the key aspects of embolotherapy with drugs, indeed an accepted advantage over intravenous drug administration, is that the drug remains in the target vascular bed. Although there is some level of uncertainty in TACE interpreting the persistence of ethiodized oil from the emulsion in the target tissue, it is recognized as a biomarker of drug distribution and treatment response[26]. It also illuminates poorly perfused areas. Taken together, these observations and the stability of ethiodized oil solution in the liver over 24 h suggest that minimal escape to the circulation is likely. This is supported by the degree of coagulative necrosis revealed by histopathologic analysis, including the vessels in the treated areas.

The histopathologic effects of reactive chemistry embolization using dichloroacetic anhydride were extensive. Considering the small amount of embolic solution used (700 µL), the extent of coagulative necrosis at both the

macroscopic and microscopic scale was remarkable. The representative H&E-stained section in Fig. 5A shows two primary lesions, and the cross section of the *smaller* lesion is approximately 3000 μm x 6600 μm. Inspection of the surrounding tissue confirms that this was not an aberrant or artifactual longitudinal measurement. In cases of such extreme damage caused by liquid embolics, it can be difficult to ascertain the center of a lesion to accurately define an effective radius of cell death. Nevertheless, this result compares extremely well against the lethal dose of beta radiation from yttrium-90 beads. Technically, beta radiation has a penetration distance of approximately 1000–2000 μm in soft tissue. However, a single number without further context does not accurately reflect the situation, as it does not account for dose at that distance. In fact, the lethal dose of beta radiation drops off very rapidly, reaching only ≈ 50 μm from the source[27].

The effective cytotoxic distance from the vessel lumen in conventional TACE has not been quantified due to the many variables involved. However, studies of DEB-TACE provide some insight and may be viewed as a best-case scenario. In animal and human studies, fluorescence imaging has been used to quantitate the drop-off in the concentration of doxorubicin over distance from the loaded beads[28,29]. At 100 μm from the beads, the doxorubicin concentration was approximately 1 mM, which is within the range for the LD_{50} of doxorubicin for many tumor cells in culture. By definition, this dose leaves fully half of the cells still viable, and this value is found under optimal conditions to express toxicity. In addition, the doxorubicin concentrations in some areas of non-necrotic tissue were similar to those in areas of necrotic tissue, calling into question the premise that doxorubicin contributes to the overall outcome. In the present study, the relatively sharp margins of such large areas of devitalized tissue and the unambiguous degree of damage suggest that, overall, reactive chemistry embolization has considerable therapeutic potential.

In this initial investigation of reactive embolization, the results of multiplex immunofluorescence microscopy were necessarily qualitative. Nevertheless, these results revealed profound differences in the spatial distribution and intensity of several markers, thereby illuminating potential mechanisms underlying the observed effects. The most striking observation was the absence of fluorescence with multiple antibodies and DAPI in large areas that corresponded to the most severe damage on H&E-stained sections. There are two possible explanations for this observation. The first is that the epitopes in these areas were either distorted or obscured owing to protein denaturation, which would have effectively nullified the epitopes. The second is that the epitopes underwent covalent modification by the reagent, dichloroacetic anhydride. Such modifications also would have disrupted the affinity of the antibodies and resulted in a loss of signal in the affected areas. This may also help explain the decreased fluorescence intensity of arginase 1 in severely affected areas. The observed difference suggests partial but not total loss of affinity for the anti–arginase 1 antibody. Vimentin staining was also absent in the damage zone, but in contrast to other biomarkers, it was more prominent in the regions surrounding the affected areas than in normal tissue. This may indicate an early fibroblast response in the surrounding tissue, but further work is needed to substantiate this notion.

The distribution of signal from CD45 also bears further comment as the pattern was clearly altered in the treated areas. When compared to healthy liver, where CD45 + cells were evenly dispersed, punctate fluorescence from CD45 was observed in areas of coagulative necrosis. These CD45 + foci were present at much lower frequency than surrounding tissue. Rather than suggesting an infiltration of viable CD45 + cells in the 24 h after the procedure, the presence of the signal despite the degree of damage strongly suggests that the particular epitope for CD45 was at least somewhat stable under the conditions. One explanation consistent with these observations is that the procedure resulted in the death of a preexisting population of CD45 + cells. The accumulation of CD45 + cells at the margin of the necrotic areas suggests an early inflammatory response, but further work is required to characterize the sub-populations in more detail. Finally, the loss of DAPI signal is noteworthy due to the well-known inherent stability of DNA under many conditions. Because DAPI intercalates into DNA, the localized loss of DAPI fluorescence implies that DNA was not stable under the reactive chemistry conditions. Given the local exotherm from the reaction and considering that acidic reaction products likely lower the local pH and that a low pH has a damaging effect on DNA structure, this finding is to be expected. Indeed, the loss of the DAPI signal might be viewed as a surrogate marker of local acidity.

As with the immunofluorescence data, MALDI-MSI revealed substantial variations in certain features in treated and adjacent undamaged healthy tissues at the molecular level with significant implications. Consistent with the immunofluorescence data, the MALDI-MSI data provide further strong evidence that additional chemical reactions beyond the expected simple hydrolysis and thermal or pH-based denaturing of proteins occurred. For any one analyte or feature in a defined area to be at an almost undetectable concentration or altogether absent implies that the conditions created by reactive embolization caused a chemical transformation of the analyte to a different species with a different mass and/or charge. Similarly, the discovery of molecular species that are not present in the surrounding tissue points to the creation of new compounds as a result of in situ chemistry. Exactly which new compound was formed in any one case would be challenging to deconvolute, but a logical approach would be to start with a structural confirmation of the existing analyte in the surrounding tissues. From there, it may be possible to consider the transformations plausible under the expected conditions of an acidic pH and a transient input of heat energy to guide further inquiry. Another intriguing possibility is that the available nucleophiles on proteins and glycans were covalently modified, as hinted at by the results of the immunofluorescence studies discussed above.

The large diameter of the lesions from a small delivered volume, the degree of damage seen histologically with cytoskeletal disruption, indeed so extreme that antibodies no longer recognize their epitopes in immunofluorescence, combined with the loss of multiple molecular ions at MSI and the appearance of new molecular species in the damaged areas, are all consistent with the interpretation that chemical changes occurred due to reaction of the anhydride in tissue. The data presented here provide the first direct evidence that reactive embolization results in fundamental changes in tissue architecture down to the molecular level, suggesting significant therapeutic potential upon optimization. However, this work raises several new questions. From a

clinical standpoint, the most immediate question is how to achieve a homogeneous distribution of the embolic material to ensure adequate treatment in a target vascular bed. The preferred technique is not yet known, but it may include administering vasodilators before the procedure and/or altering the rate of delivery, the concentration of the reagent, choice of reagent, and/or how the reagent is formulated. This work establishes a baseline for future research involving tumors by providing a basis for comparison with and perhaps as a viable alternative to established methods such as TACE. Additional studies in large animal models are needed to further clarify these questions. Basic science studies are needed to investigate the extensive implications of localized covalent modification made possible using image-guided techniques. The candidate reagents in this chemical space are myriad, as are the parameters and conditions of their delivery. These factors and the encouraging results presented here open a wide new field of investigation with image-guided in vivo chemistry that is worthy of further exploration.

Methods

Animal care and use

The study was conducted under protocol 00001478-RN03, which was approved by MD Anderson's Institutional Animal Care and Use Committee in August 2024. All methods were performed in accordance with the relevant guidelines and regulations and conducted in accordance with ARRIVE guidelines. Three female outbred swine (30–35 kg; Oakhill Genetics, Ewing, Illinois) were acclimated under approved housing conditions according to institutional guidelines. Anesthesia was induced with an intramuscular injection of tiletamine hydrochloride and zolazepam (Zoetis US, Parsippany, NJ, USA). This was followed by intubation, and general anesthesia was maintained with isoflurane (2–4% to effect). Animals were in the dorsal recumbent position during the procedure and in the lateral decubitus position during recovery. Post-procedure pain and swelling were managed with once-daily oral meloxicam (0.4 mg/kg; Boehringer Ingelheim, Ingelheim am Rhein, Germany).

Reagents and materials

Dichloroacetic anhydride (Fujifilm WAKO Chemicals USA, Richmond, VA, USA) and ethiodized oil (Lipiodol, Guerbet, Princeton, NJ, USA) were used directly as supplied. Iodinated contrast (Visipaque 320, GE Healthcare, Milwaukee, WI, USA) was administered intravenously for whole-body scanning or intraarterially for angiography. 9-aminoacridine (Sigma Aldrich, St. Louis, MO, USA) was used as the matrix for mass spectrometry imaging.

Imaging

Computed tomography (CT) and fluoroscopy were performed in a hybrid suite. This included a Definition Edge scanner and a ceiling-mounted Artis-Q imaging system (Siemens Healthineers, Forchheim, Germany) using a frame rate of up to 7 frames per second for digital subtraction angiography. Triple-phase CT (without contrast, arterial phase, portal venous phase) was performed before the procedure to acquire baseline images, immediately after the procedure to document the distribution of the embolic agent, and 24 h after the procedure to evaluate the distribution of the embolic agent for stability over time. Image reconstruction was performed at slice thicknesses of 0.5 mm and 3 mm. Post-processing for multiplanar reformatting and volume rendering was performed using the OsiriX MD software program (version 14.0.1, Pixmeo, Geneva, Switzerland).

Reactive embolization

Under ultrasound guidance, an introducer sheath was placed using the Seldinger technique in the common femoral artery. Through this sheath, a 5 F Sos-2 base catheter (Cook Medical, Bloomington, IN, USA) was advanced to the origin of the celiac artery, and arteriography of the celiac artery and branch vessels was performed. Through the base catheter, a 2.8 F Renegade Hi-Flo microcatheter and Fathom 0.016 guidewire (both from Boston Scientific, Marlborough, MA, USA) were coaxially advanced into the arterial tree in the liver. The microcatheter was situated in the desired position for magnified angiography of hepatic lobar vessels and the delivery of the reactive embolic solution. The freshly prepared solution (2 mol/L dichloroacetic anhydride in ethiodized oil) was delivered in small aliquots to a total of 700 µL through the microcatheter under direct fluoroscopic visualization. Completion angiography was performed to document the level of occlusion of the lobar hepatic artery. The catheters and sheath were removed, and hemostasis was achieved with manual compression.

Pathology and immunohistochemistry

Immediately following the final CT imaging, euthanasia was performed with an overdose of Beuthanasia delivered intravenously. At necropsy the liver was removed en bloc and photographed. CT of the explanted organ was then performed to help correlate imaging findings with histopathological findings. Tissue specimens were removed, photographed, and fixed in 10% formalin for subsequent paraffin embedding. Sections of the specimens were mounted on slides and stained with hematoxylin and eosin (H&E) or processed for immunohistochemical studies. Additional sections were snap-frozen in liquid nitrogen for mass spectrometry (described below).

For multiplex immunofluorescence microscopy, 4-µm-thick sections were stained using a Bond RX autostainer (Leica Biosystems, Deer Park, IL, USA) and an Opal 7-color IHC detection kit (Akoya Biosciences, Marlborough, MA, USA). The sections were evaluated using DAPI (for nuclear staining) in conjunction with antibodies against CD31 (endothelium), smooth muscle actin, CD45 (leukocytes), vimentin (mesenchymal cells), cleaved caspase-3 (apoptosis), and arginase 1 (hepatocytes). The sections were imaged using a Versa 8 whole slide scanner (Leica Biosystems).

Matrix-assisted laser desorption ionization mass spectrometry imaging

Matrix-assisted laser desorption ionization mass spectrometry imaging (MALDI-MSI) data were acquired in a fashion similar to that reported previously[30]. Briefly, after application of matrix, scans of frozen sections were obtained in negative ionization mode using a SYNAPT G2-Si mass spectrometer (Waters Corporation, Milford, MA, USA) at a 60-µm spot size with 100-µm spacing. The matrix was 9-aminoacridine, which was applied using an M5 Sprayer (HTX Technologies, LLC, Chapel Hill, NC, USA). The mass range was set at m/z 50–1200, and the instrument was calibrated using peak signals from red phosphorus. Image reconstruction was done with the High-Definition Imaging software program (version 1.4, Waters Corporation).

Data availability

The datasets generated during and/or analysed during the current study are available from the corresponding author on reasonable request and completion of a materials transfer agreement per institutional policy.

Received: 15 December 2024; Accepted: 13 May 2025
Published online: 19 May 2025

References

1. Lang, S. et al. Hepatocellular carcinoma surveillance with liver imaging is not associated with improved survival. *Scand. J. Gastroenterol.* **55**, 222–227. https://doi.org/10.1080/00365521.2020.1718747 (2020).
2. Pfister, D. et al. NASH limits anti-tumour surveillance in immunotherapy-treated HCC. *Nature* **592**, 450–456. https://doi.org/10.1038/s41586-021-03362-0 (2021).
3. Kudo, M. et al. IMbrave150: efficacy and safety of Atezolizumab plus bevacizumab versus Sorafenib in patients with Barcelona clinic liver Cancer stage B unresectable hepatocellular carcinoma: an exploratory analysis of the phase III study. *Liver Cancer*. **12**, 238–250. https://doi.org/10.1159/000528272 (2023).
4. Fulgenzi, C. A. M. et al. Immunotherapy vs best supportive care for patients with hepatocellular Cancer with Child-Pugh B dysfunction. *JAMA Oncol.* **10**, 1253–1258. https://doi.org/10.1001/jamaoncol.2024.2166 (2024).
5. Fulgenzi, C. A. M. et al. New frontiers in the medical therapy of hepatocellular carcinoma. *Chemotherapy* **67**, 164–172. https://doi.org/10.1159/000521837 (2022).
6. Huang, Y. & Yu, W. Advances in immune checkpoint therapy in hepatocellular carcinoma. *Br. J. Hosp. Med. (Lond).* **85**, 1–21. https://doi.org/10.12968/hmed.2024.0375 (2024).
7. Llovet, J. M. et al. Immunotherapies for hepatocellular carcinoma. *Nat. Rev. Clin. Oncol.* **19**, 151–172. https://doi.org/10.1038/s41571-021-00573-2 (2022).
8. Kudo, M. Lack of response to immunotherapy in non-alcoholic steatohepatitis related hepatocellular carcinoma. *Hepatobiliary Surg. Nutr.* https://doi.org/10.21037/hbsn-21-203 (2021).
9. Cabibbo, G., Celsa, C., Alimenti, E. & Iavarone, M. Evaluating the risk-benefit ratio of immunotherapy according to liver-functional reserve in advanced HCC: the dark side of the Moon. *Hepatology* **77**, 1074–1077. https://doi.org/10.1097/HEP.0000000000000205 (2023).
10. Guiu, B., Garin, E., Allimant, C., Edeline, J. & Salem, R. TARE in hepatocellular carcinoma: from the right to the left of BCLC. *Cardiovasc. Intervent Radiol.* **45**, 1599–1607. https://doi.org/10.1007/s00270-022-03072-8 (2022).
11. Garin, E., Guiu, B., Edeline, J., Rolland, Y. & Palard, X. Trans-arterial radioembolization dosimetry in 2022. *Cardiovasc. Intervent Radiol.* **45**, 1608–1621. https://doi.org/10.1007/s00270-022-03215-x (2022).
12. Reig, M. et al. BCLC strategy for prognosis prediction and treatment recommendation: the 2022 update. *J. Hepatol.* **76**, 681–693. https://doi.org/10.1016/j.jhep.2021.11.018 (2022).
13. Letzen, B. S. et al. Lipiodol as an intra-procedural imaging biomarker for liver tumor response to transarterial chemoembolization: Post-hoc analysis of a prospective clinical trial. *Clin. Imaging.* **78**, 194–200. https://doi.org/10.1016/j.clinimag.2021.05.007 (2021).
14. Gaba, R. C. et al. Ethiodized oil uptake does not predict doxorubicin drug delivery after chemoembolization in VX2 liver tumors. *J. Vasc Interv Radiol.* **23**, 265–273. https://doi.org/10.1016/j.jvir.2011.10.022 (2012).
15. Gjoreski, A. et al. Single-center randomized trial comparing conventional chemoembolization versus doxorubicin-loaded polyethylene glycol microspheres for early- and intermediate-stage hepatocellular carcinoma. *Eur. J. Cancer Prev.* **30**, 258–266. https://doi.org/10.1097/CEJ.0000000000000623 (2021).
16. Massani, M., Stecca, T., Ruffolo, C. & Bassi, N. Should we routinely use DEBTACE for unresectable HCC? cTACE versus DEBTACE: a single-center survival analysis. *Updates Surg.* **69**, 67–73. https://doi.org/10.1007/s13304-017-0414-3 (2017).
17. Brown, K. T. et al. Randomized trial of hepatic artery embolization for hepatocellular carcinoma using Doxorubicin-Eluting microspheres compared with embolization with microspheres alone. *J. Clin. Oncol.* **34**, 2046–2053. https://doi.org/10.1200/JCO.2015.64.0821 (2016).
18. Shirono, T. et al. Durable complete response is achieved by balloon-occluded transcatheter arterial chemoembolization for hepatocellular carcinoma. *Hepatol. Commun.* **6**, 2594–2604. https://doi.org/10.1002/hep4.2016 (2022).
19. Lucatelli, P. et al. Long-Term outcomes of balloon TACE for HCC: an European multicentre Single-Arm retrospective study. *Cardiovasc. Intervent Radiol.* **47**, 1074–1082. https://doi.org/10.1007/s00270-024-03779-w (2024).
20. Jing, C. et al. Therapeutic analysis of 632 cases treated by transcatheter arterial chemoembolization combined with ablation in hepatocellular carcinoma: A retrospective study. *Eur. J. Radiol.* **178**, 111619. https://doi.org/10.1016/j.ejrad.2024.111619 (2024).
21. Brown, Z. J., Hewitt, D. B. & Pawlik, T. M. Combination therapies plus transarterial chemoembolization in hepatocellular carcinoma: a snapshot of clinical trial progress. *Expert Opin. Investig. Drugs.* **31**, 379–391. https://doi.org/10.1080/13543784.2022.2008355 (2022).
22. Radovitch, H. et al. Influence of the radiological response on histological necrosis and on the survival of patients treated with transarterial chemoembolization for hepatocellular carcinoma secondary to cirrhosis on the liver transplantation waiting list. *Transpl. Proc.* **56**, 1774–1783. https://doi.org/10.1016/j.transproceed.2024.08.033 (2024).
23. Mosenthal, M. et al. Locoregional therapies for hepatocellular carcinoma prior to liver transplant: comparative pathologic necrosis, radiologic response, and recurrence. *J. Vasc Interv Radiol.* **35**, 506–514. https://doi.org/10.1016/j.jvir.2023.12.009 (2024).
24. Sarwar, A. et al. Factors associated with complete pathologic necrosis of hepatocellular carcinoma on explant evaluation after locoregional therapy: A National analysis using the UNOS database. *AJR Am. J. Roentgenol.* **220**, 727–735. https://doi.org/10.2214/AJR.22.28385 (2023).
25. Kankotia, S. & Stacpoole, P. W. Dichloroacetate and cancer: new home for an orphan drug? *Biochim. Biophys. Acta*. **1846**, 617–629. https://doi.org/10.1016/j.bbcan.2014.08.005 (2014).
26. Mendiratta-Lala, M. et al. Ethiodized oil as an imaging biomarker after conventional transarterial chemoembolization. *Eur. Radiol.* **34**, 3284–3297. https://doi.org/10.1007/s00330-023-10326-7 (2024).

27. Gulec, S. A., Sztejnberg, M. L., Siegel, J. A., Jevremovic, T. & Stabin, M. Hepatic structural dosimetry in (90)Y microsphere treatment: a Monte Carlo modeling approach based on lobular microanatomy. *J. Nucl. Med.* **51**, 301–310. https://doi.org/10.2967/jnumed.109.069278 (2010).
28. Namur, J. et al. Embolization of hepatocellular carcinoma with drug-eluting beads: doxorubicin tissue concentration and distribution in patient liver explants. *J. Hepatol.* **55**, 1332–1338. https://doi.org/10.1016/j.jhep.2011.03.024 (2011).
29. Namur, J. et al. Drug-eluting beads for liver embolization: concentration of doxorubicin in tissue and in beads in a pig model. *J. Vasc Interv Radiol.* **21**, 259–267. https://doi.org/10.1016/j.jvir.2009.10.026 (2010).
30. Guo, C., Baluya, D. L., Thompson, E. A., Whitley, E. M. & Cressman, E. N. K. Correlation of molecular and morphologic effects of thermoembolization in a swine model using mass spectrometry imaging. *J. Mass. Spectrom.* **55**, e4477. https://doi.org/10.1002/jms.4477 (2020).

Acknowledgements
We thank Joe Munch in MD Anderson's Research Medical Library for editing the manuscript and Emily Thompson PhD for CT image acquisition. We would like to thank the John S. Dunn Foundation, the Wiegand Foundation and Archer Foundation for support of instrumentation.

Author contributions
Conceptualization, E.C. methodology, E.C.; software, E.C., D.F; validation, E.C., D.S.; formal analysis, E.C., D.S., S.W., D.F.; investigation, E.C., D.S., S.W., N.F.; D.F.; resources, E.C.; data curation, E.C., D.S., N.F; D.F.; writing—original draft preparation, E.C.; writing—review and editing, E.C., D.S., S.W.; N.F.; D.F.; visualization, E.C., D.S., D.F.; supervision, E.C.; project administration, E.C.; funding acquisition, E.C.

Declarations

Competing interests
The authors declare no competing interests.

Additional information
Supplementary Information The online version contains supplementary material available at https://doi.org/10.1038/s41598-025-02376-2.

Correspondence and requests for materials should be addressed to E.C.

Reprints and permissions information is available at www.nature.com/reprints.

Publisher's note Springer Nature remains neutral with regard to jurisdictional claims in published maps and institutional affiliations.